

---

---

MATHEMATICAL  
PHYSICS

---

---

# Quasi-Gasdynamics Model and Numerical Algorithm for Describing Mixtures of Different Fluids

T. G. Elizarova<sup>a,\*</sup> and E. V. Shil'nikov<sup>a,\*\*</sup>

<sup>a</sup> Federal Research Center Keldysh Institute of Applied Mathematics, Russian Academy of Sciences,  
Moscow, 125047 Russia

\*e-mail: telizar@mail.ru

\*\*e-mail: shilnikov@imamod.ru

Received November 14, 2022; revised November 14, 2022; accepted March 30, 2023

**Abstract**—An elegant and easy-to-implement numerical algorithm for simulating flows of homogeneous gas mixtures with component temperatures and velocities assumed to be equal is constructed and tested. The algorithm yields monotone density profiles for the components even if their specific heat ratios are widely different. The algorithm can be used to simulate some flows of gas–liquid mixtures.

**Keywords:** homogeneous gas mixture, one-fluid approximation, finite-difference algorithm, regularized equations

**DOI:** 10.1134/S0965542523070059

## INTRODUCTION

Numerical simulation of the behavior of different fluids and, in particular, gas–gas and gas–liquid mixtures in various flow regimes is important for many domains of science and engineering, including problems of current interest related to the manufacturing of components for microelectronic devices. Due to its relative simplicity for practical applications, the description of homogeneous mixtures in the one-fluid approximation especially in demand. By homogeneous mixtures, we mean ones in which there are no specific identification of interfaces between the components.

In the one-fluid approximation, the velocities and temperatures of the mixture components are assumed to be in thermodynamic equilibrium. A wide variety of corresponding systems of equations can be found in numerous monographs (see, e.g., [1–3]). In two-fluid models of mixtures, the components of the mixture are assumed to have individual macroscopic velocities and temperatures, which leads to a significantly more complicated mathematical model of the process with an increased number of equations in the system. Additionally, we need to take into account exchange terms in the momentum and energy equations, which account for the interaction between the components of the mixture. The description of such mixtures is also much bulkier from an algorithmic point of view. At the same time, the applicability of such models is significantly limited by the applicability of continuum models for nonequilibrium flows (see, e.g., [4]). Knudsen numbers at which gases can be described in the two-fluid approximation correspond to moderately rarefied gas flows and belong to a rather narrow range of values. In this paper, our consideration is restricted to the one-fluid approximation for describing homogeneous mixtures of fluids.

Numerical algorithms for describing homogeneous one-fluid mixtures are abundant, differing in the original system of equations and its numerical implementation. Specifically, algorithms for gas mixture simulation based on regularized, or quasi-gasdynamics (QGD) equations in one-temperature and one-speed approximations for the mixture were described and tested in [5–7]. The first variant of such a system for rarefied flows was proposed in [4].

However, numerical computations have shown that mixture flows with widely different ratios of specific heats simulated by applying this approach give rise to spurious oscillations of the component densities, while the total mixture density remains rather smooth (see [7, 8]). In particular, spurious oscillations of component densities can lead to negative density values in low-density regions. A similar difficulty arises in using other numerical algorithms. Eliminating this shortcoming results in significantly more complicated numerical schemes (see [9–12]). For example, in [9, 12], this shortcoming was eliminated by

applying the double flux method, in which special modifications of numerical techniques are used to approximate convective fluxes at cell boundaries.

A new variant of regularized, or QGD equations for a gas mixture in two- and one-fluid approximations satisfying the entropy nondecrease condition for the mixture was proposed recently in [13]. The equations for the one-fluid approximation are constructed by aggregating the equations for the two-fluid model. Entropy-consistent difference schemes based on these equations were found applicable to problems with large differences between component pressures and densities, ensuring that they are nonnegative. However, the resulting algorithm is rather complicated because of the use of a special averaging of flow variables in the computation of fluxes at cell boundaries.

In this paper, for the first time, we construct and test an elegant and easy-to-implement QGD algorithm for simulating homogeneous gas mixture flows, assuming that the temperatures and velocities of the components are identical. The algorithm yields monotone density profiles for the components even if their ratios of specific heats are widely different. A variant of the algorithm has recently been incorporated into the open-source OpenFOAM package (see [14]). The implementation of the QGD solver for a one-component gas within the OpenFOAM platform is described in [15].

In the last section of this paper, we show that an algorithm similar in structure can be used to simulate a class of problems concerning the interaction of significantly different fluids, namely, gas–liquid interactions. Equations of state are used for both fluids, but a simplified Van der Waals equation of state is applied for the liquid component.

As an example, the algorithm is used to solve one-dimensional Riemann problems, which clearly demonstrate the features, advantages, and limitations of the described approach.

## 1. SYSTEM OF EQUATIONS FOR TWO-COMPONENT GAS IN THE ONE-FLUID APPROXIMATION

In the one-fluid model, a gas mixture is assumed to have a unified velocity  $\mathbf{u}$  and a unified temperature  $T$ , while the density, pressure, specific total energy, and other parameters of the mixture are determined in terms of the parameters of its components as

$$\rho = \rho_a + \rho_b, \quad p = p_a + p_b.$$

The equations of state of the components are

$$p_k = \rho_k R_k T, \quad \varepsilon_k = C_{vk} T, \quad k = a, b. \quad (1)$$

Here,  $R_k$  and  $\varepsilon_k$  are the gas constant and the specific internal energy of a mixture component, respectively. The parameters of the mixture are computed as weighted values in the form

$$\begin{aligned} R &= \frac{R_a \rho_a + R_b \rho_b}{\rho} = C_p - C_v, \quad \gamma = \frac{C_p}{C_v}, \quad \gamma - 1 = \frac{R}{C_v}, \\ \varepsilon &= \frac{\varepsilon_a \rho_a + \varepsilon_b \rho_b}{\rho}, \quad C_v = \frac{C_{va} \rho_a + C_{vb} \rho_b}{\rho}. \end{aligned} \quad (2)$$

The total energy is given by

$$E = \rho \varepsilon + \rho \frac{\mathbf{u}^2}{2}.$$

The speed of sound in the mixture of gases  $a$  and  $b$  is calculated using the formula

$$\rho c_s^2 = \gamma_a p_a + \gamma_b p_b. \quad (3)$$

Following [3–8], the original system of equations governing the homogeneous mixture of two gases is chosen in the form

$$\frac{\partial \rho_a}{\partial t} + \operatorname{div}(\rho_a \mathbf{u}) = 0, \quad (4)$$

$$\frac{\partial \rho_b}{\partial t} + \operatorname{div}(\rho_b \mathbf{u}) = 0, \quad (5)$$

$$\frac{\partial \rho \mathbf{u}}{\partial t} + \operatorname{div}(\rho \mathbf{u} \otimes \mathbf{u}) + \nabla p = \operatorname{div} \Pi + \rho \mathbf{F}, \quad (6)$$

$$\frac{\partial E}{\partial t} + \operatorname{div}((E + p)\mathbf{u}) = -\operatorname{div} \mathbf{q} + \operatorname{div}(\Pi \cdot \mathbf{u}) + \rho \mathbf{u} \cdot \mathbf{F} + Q. \tag{7}$$

Here,  $\mathbf{F}$  and  $Q$  denote the specific intensities of external forces and heat sources, respectively.

The Navier–Stokes viscous stress tensor  $\Pi_{\text{NS}}$  in the form of Newton’s shear stress law and the heat flux  $\mathbf{q}_{\text{NS}}$  in the form of Fourier’s law have the traditional form:

$$\Pi_{\text{NS}} = \mu \left( (\nabla \otimes \mathbf{u}) + (\nabla \otimes \mathbf{u})^T - \frac{2}{3} I \operatorname{div} \mathbf{u} \right), \quad \mathbf{q}_{\text{NS}} = -\kappa \nabla T,$$

where  $I$  is the identity matrix and  $\mu$  and  $\kappa$  are the dynamic viscosity and thermal conductivity of the mixture.

## 2. CONSTRUCTION OF REGULARIZED EQUATIONS FOR THE GAS MIXTURE

To construct a regularized version of the original system, we use a procedure for smoothing flow variables over a short time interval (see, e.g., [16]). A similar averaging of the gasdynamic equations over a small volume yields regularized gasdynamic equations, which can be found in [4, 17]. Following [16], we average the system of equations over a short time interval  $\Delta t$  and assume that the system of equations has a sufficiently smooth solution. Applying the mean-value theorem to evaluate integrals with respect to time and assuming that the averaging interval is rather short, we represent the variations in the gas parameters over the interval time  $\Delta t \sim \tau$  as the first term of the Taylor series expansion:

$$\tilde{\rho}_a = \rho_a + \tau \frac{\partial \rho_a}{\partial t}, \quad \tilde{\rho}_b = \rho_b + \tau \frac{\partial \rho_b}{\partial t}, \quad \tilde{\rho} = \rho + \tau \frac{\partial \rho}{\partial t}, \quad \tilde{p} = p + \tau \frac{\partial p}{\partial t}, \quad \tilde{\mathbf{u}} = \mathbf{u} + \tau \frac{\partial \mathbf{u}}{\partial t}.$$

After substituting these expansions into the original equations (4)–(7), the first equation of the system becomes

$$\frac{\partial \tilde{\rho}_a}{\partial t} + \operatorname{div}(\tilde{\rho}_a \tilde{\mathbf{u}}) = 0. \tag{8}$$

To compute the averaged values in Eq. (8), the time derivatives are transformed using the original equations (4) and (6). Combining Eqs. (4) and (5) with definitions (1) yields the following equation for the total mixture density:

$$\frac{\partial \rho}{\partial t} + \operatorname{div}(\rho \mathbf{u}) = 0. \tag{9}$$

Then the momentum equation (6), combined with Eq. (9), is transformed into nonconservative form:

$$\frac{\partial \mathbf{u}}{\partial t} + \mathbf{u} \operatorname{div} \mathbf{u} + \frac{1}{\rho} \nabla p = \frac{1}{\rho} \operatorname{div} \Pi + \mathbf{F}. \tag{10}$$

Dropping the viscous terms from Eq. (10), we find the velocity derivative  $\frac{\partial \mathbf{u}}{\partial t}$ .

Then, in the averaged equation (8),

$$\tilde{\rho}_a \tilde{\mathbf{u}} = (\rho_a - \tau \operatorname{div}(\rho_a \mathbf{u})) \left( \mathbf{u} - \tau \left( \mathbf{u} \operatorname{div} \mathbf{u} + \frac{1}{\rho} \nabla p - \mathbf{F} \right) \right).$$

This determines a regularizing addition to the regularized equation (8) for the density of component  $a$ . The form of the additions in the momentum and energy equations remains the same as for the QGD equations for a one-component gas. The details of this procedure can be found in [16].

The resulting regularized system of equations for describing the flow of two gases is given by

$$\frac{\partial \rho_a}{\partial t} + \operatorname{div}(\rho_a (\mathbf{u} - \hat{\mathbf{w}})) = \nabla(\tau \mathbf{u} \cdot \operatorname{div}(\rho_a \mathbf{u})), \tag{11}$$

$$\frac{\partial \rho_b}{\partial t} + \operatorname{div}(\rho_b (\mathbf{u} - \hat{\mathbf{w}})) = \nabla(\tau \mathbf{u} \cdot \operatorname{div}(\rho_b \mathbf{u})), \tag{12}$$

$$\frac{\partial \rho \mathbf{u}}{\partial t} + \operatorname{div}(\rho (\mathbf{u} - \mathbf{w}) \otimes \mathbf{u}) + \nabla p = \operatorname{div} \Pi + (\rho - \tau \operatorname{div}(\rho \mathbf{u})) \mathbf{F}, \tag{13}$$

$$\frac{\partial E}{\partial t} + \operatorname{div}((E + p)(\mathbf{u} - \mathbf{w})) = -\operatorname{div} \mathbf{q} + \operatorname{div}(\Pi \cdot \mathbf{u}) + \rho(\mathbf{u} - \mathbf{w}) \cdot \mathbf{F} + Q. \quad (14)$$

The auxiliary QGD quantities are small additions to the velocity, viscous stress tensor, and heat flux and have the form

$$\mathbf{w} = \frac{\tau}{\rho}(\operatorname{div}(\rho \mathbf{u} \otimes \mathbf{u}) + \nabla p - \rho \mathbf{F}) = \hat{\mathbf{w}} + \frac{\tau}{\rho} \mathbf{u} \operatorname{div}(\rho \mathbf{u}), \quad (15)$$

$$\hat{\mathbf{w}} = \frac{\tau}{\rho}(\rho(\mathbf{u} \nabla) \mathbf{u} + \nabla p - \rho \mathbf{F}), \quad (16)$$

$$\mathbf{q} = \mathbf{q}_{\text{NS}} + \mathbf{q}^\tau, \quad -\mathbf{q}^\tau = \tau \rho \mathbf{u} \left( \mathbf{u} c_V \nabla T + p(\mathbf{u} \nabla) \left( \frac{1}{\rho} \right) - \frac{Q}{\rho} \right), \quad (17)$$

$$\Pi = \Pi_{\text{NS}} + \rho \mathbf{u} \otimes \hat{\mathbf{w}} + \tau(\mathbf{u} \nabla p + \gamma p \operatorname{div} \mathbf{u} - (\gamma - 1)Q). \quad (18)$$

Summing Eqs. (11) and (12) yields a regularized continuity equation of the QGD system for a one-component gas, namely,

$$\frac{\partial \rho}{\partial t} + \operatorname{div} \rho(\mathbf{u} - \mathbf{w}) = 0.$$

System (11)–(14) differs from the one used in [6–8] primarily in the method for computing the QGD additions in the continuity equations for the components. It is this modification that ensures no oscillations behind the contact discontinuity in the numerical experiments. Other modifications, such as the replacement of  $\nabla \varepsilon$  by  $C_V \nabla T$  in (19), are less important, although they also improve the quality of the numerical solution.

The regularization parameter is related to the spatial mesh size  $h$  and the speed of sound in the mixture by the formula

$$\tau = \alpha \frac{h}{c_s}. \quad (19)$$

In solving the Euler equations, the viscosity  $\mu$  and the thermal conductivity  $\kappa$  of the mixture are treated as artificial regularizers and are computed as

$$\mu = \tau p \operatorname{Sc}, \quad \kappa = \frac{\mu C_p}{\operatorname{Pr}}. \quad (20)$$

Thus, there are three free numerical parameters for tuning the dissipation properties of the algorithm: the coefficient  $\alpha$ , the Schmidt number  $\operatorname{Sc}$ , and the Prandtl number  $\operatorname{Pr}$ . The baseline values are  $\alpha = 0.5$  and  $\operatorname{Sc} = \operatorname{Pr} = 1$ .

A numerical algorithm for computing gas mixture flows on an orthogonal grid is constructed directly via a difference approximation of system (11)–(19) with the use of central differences for all spatial derivatives. Thus, the scheme has the second order of accuracy. The use of dissipative coefficients of form (19) and (20), which are proportional to the mesh size  $h$ , reduces the order of approximation of the equations to the first. Note that the additional dissipation of the scheme is strongly nonlinear and depends substantially on the solution of the problem, automatically adjusting to it. A time-explicit conditionally stable difference scheme was used in the computations.

In the computations presented below, the external force  $\mathbf{F}$  and the heat sources  $Q$  were set to zero.

### 3. RIEMANN PROBLEM FOR TWO DIFFERENT GASES

As a first example of numerical simulation, we solved the Riemann problem for two different gases. The formulation of the problem follows [12]. The details of the problem formulation and numerical results for the simplified regularization from [6] can be found in [8].

The initial conditions in the left and right parts of the domain  $0 \leq x \leq 1$  differ not only in the pressure, density, and gas velocity, but also in the properties of the gases, which are air (gas  $a$ ) and helium (gas  $b$ ). The corresponding characteristics are given in Table 1.

Figure 1 presents the numerical results for this problem in the form of density distributions for components  $a$  and  $b$  and their total density calculated by applying the techniques from [6] and system (11)–(14).

**Table 1.** Initial values of mixture parameters in the Riemann problem

Domain	$\rho_{\text{He}}$	$\rho_{\text{Air}}$	$U$	Molecular mass	$P$	$\gamma$
$0 \leq x \leq 0.5$	14.54903	0.0	0.0	He, 4.003	$10^7$	5/3
$0.5 \leq x \leq 1$	0.0	1.16355	0.0	Air, 28.96	$10^5$	7/5

It can be seen that the results based on [6] exhibit strong oscillations in the component densities and negative density values for gas  $b$ . The results based on system (11)–(14) are free of these drawbacks (Fig. 1b).

The numerical results were obtained on a uniform grid of 400 cells with the regularization parameters  $\alpha = 0.13$  and  $Sc = Pr = 1$ . The Courant number was  $\beta = 0.2$ . The computations were carried out until the time  $t_{\text{fin}} = 2.0 \times 10^{-4}$ .

As a second example, we solved a variant of Sod’s problem with a large pressure difference at the interface between the components; its formulation is described in [9, 13]. At the initial time, the discontinuity is located at the point  $x = 0.5$ , separating gas mixtures  $a$  and  $b$  as in the preceding problem with parameters  $\gamma_a = 1.4$ ,  $C_{V_a} = 1$  and  $\gamma_b = 1.6$ ,  $C_{V_b} = 1$ . The velocity of the mixture is  $u_{\text{beg}} = 0$ . For  $x < 0.5$ , the component densities are  $\rho_a = 1$ ,  $\rho_b = 0$  and the component pressures are  $p_a = 500$ ,  $p_b = 0$ . To the right of the discontinuity (for  $x > 0.5$ ), the densities are  $\rho_a = 0$ ,  $\rho_b = 1$ , and the pressures are  $p_a = 0$ ,  $p_b = 0.2$ . Thus, the pressure of the mixture to the left of the discontinuity is 2500 times higher than that to the right of the discontinuity. In the entire computational domain, the temperature is computed from the equations of state.

The computations were carried until the time  $t_{\text{fin}} = 0.011$  with the following parameters of the scheme:  $\alpha = 0.4$ ,  $\beta = 0.2$ ,  $Sc = 1$ , and  $Pr = 4$ . The numerical results obtained on three spatial grids ( $N = 500, 2000$ , and 4000) are compared in Fig. 2, which clearly shows the basic gasdynamic features of the flow and the convergence of the method under the mesh refinement. The solution obtained on the coarse grid is smoothed out. For 2000 and 4000 grid nodes, the differences in the profiles become insignificant. The numerical results agree well with the reference data from [9, 13].

By choosing suitable tuning parameters for the algorithm, we can find an optimal numerical solution. An increase in  $\alpha$  leads to a smoothing out of the discontinuities, variations in the Schmidt number  $Sc$  in the range 0.1–10 nearly does not affect the numerical result, while an increase in the Prandtl number  $Pr$  from 1 to 4 slightly changes the shape of the temperature profile near the contact discontinuity. A small defect in the velocity profile near the point  $x = 0.6$  reflects the entropy wake in the contact discontinuity zone introduced by the used difference algorithm. In the case of an entropy-consistent algorithm (see [13]), this defect of the scheme becomes nearly indistinguishable.

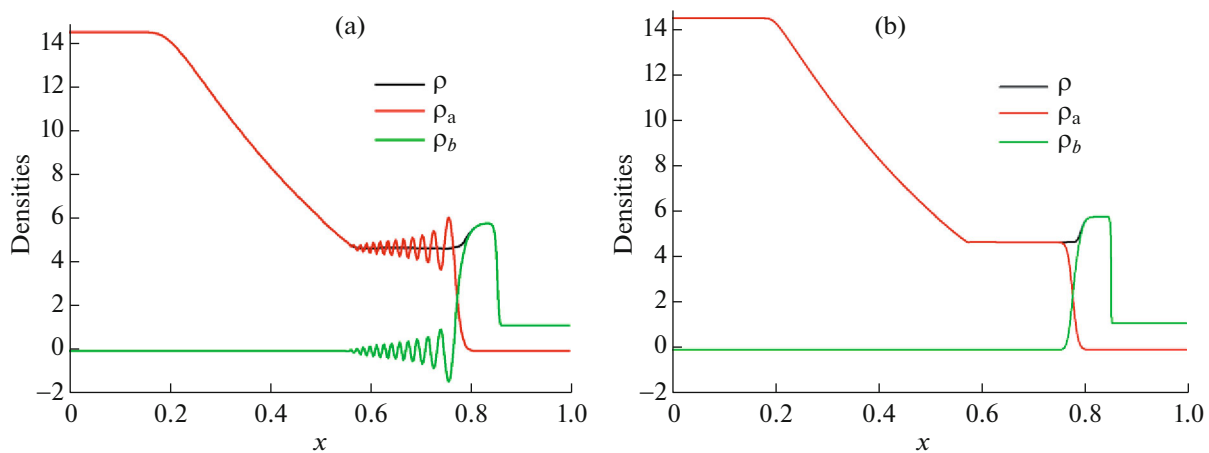


**Fig. 1.** Numerical results produced by (a) the scheme from [6] and (b) the present scheme.

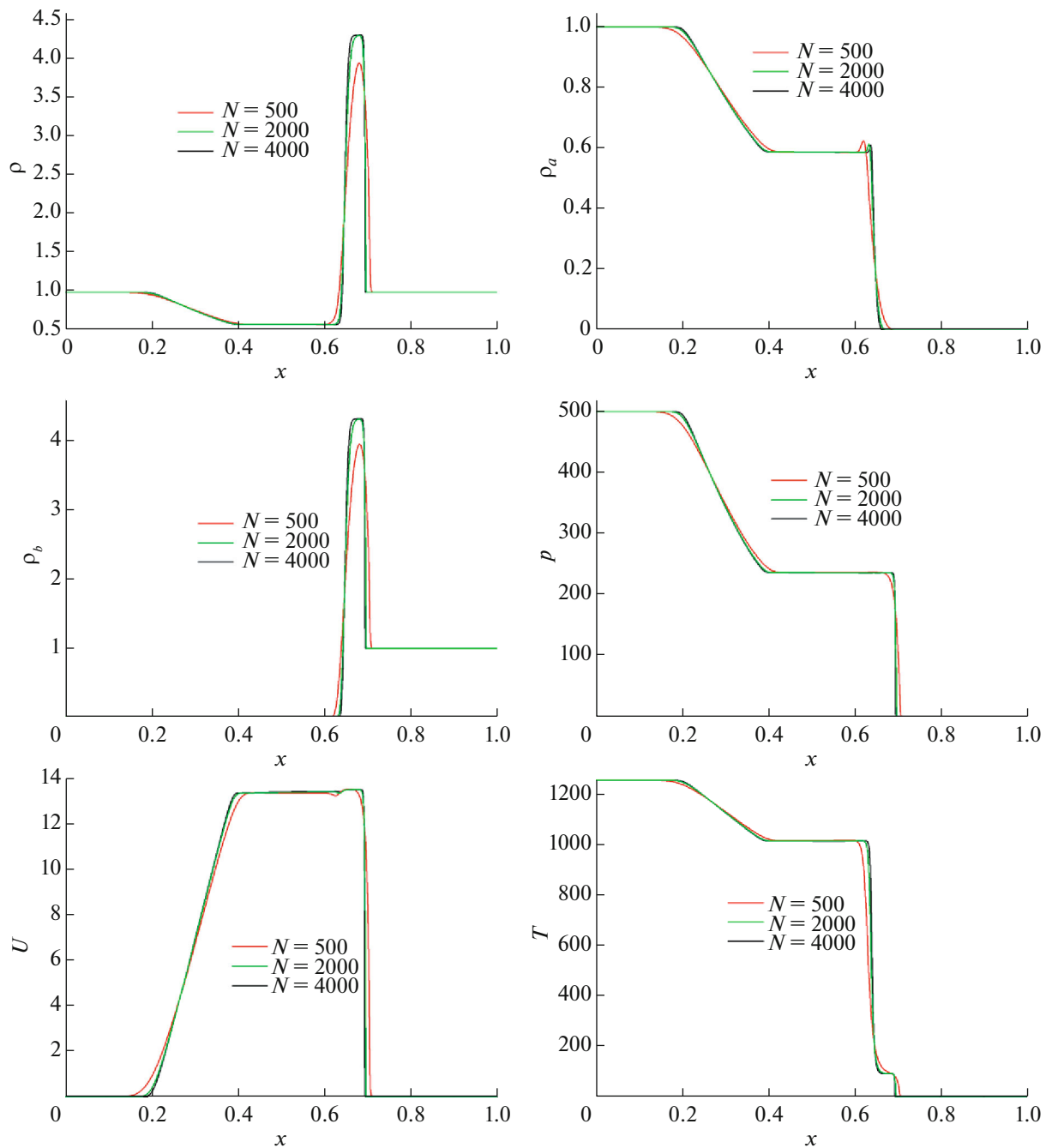


Fig. 2. Numerical results for Sod's problem with a large pressure difference.

#### 4. SHOCK INTERACTION WITH A GAS–GAS INTERFACE

Consider the problem of shock interaction with an interface between gases with widely different ratios of specific heats (see [10, 11]).

The interface is initially located at the point  $x = 0.5$ , separating the materials with  $\gamma_a = 1.35$  and  $C_{v_a} = 2.4$  on the left and with  $\gamma_b = 5.0$  and  $C_{v_b} = 1.5$  on the right. These values approximately correspond to high explosives (material  $a$ ) and confining materials (material  $b$ ). Initially, to the left of the interface at  $x = 0.1$  in material  $a$ , there is a shock wave moving to the right with velocity 2.3238 relative to the interface. At the time  $t = 0.1721$ , the shock wave collides with the interface. As a result, the transmitted shock wave propagates rightward in material  $b$ , while the reflected wave propagates leftward in material  $a$ . Figure 3 presents

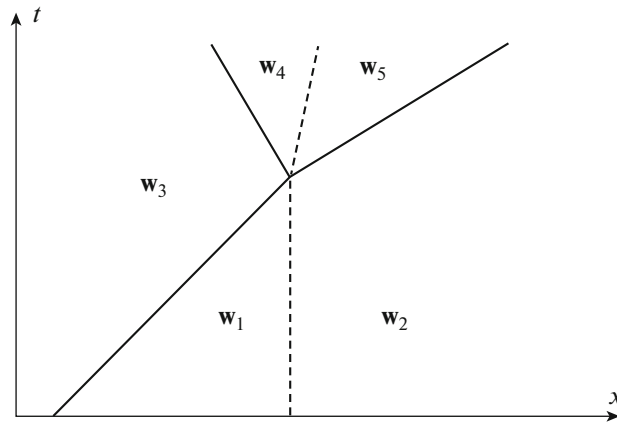


Fig. 3. The  $x-t$  diagram for the problem of the shock–interface interaction according to [10].

the  $x-t$  diagram for this problem, which shows the positions of the shock waves and the interface separating the states with constant values of the flow variables.

Table 2 lists the values of the flow parameters in the domains shown in Fig. 3. The value  $\phi_a = 0$  means that this domain contains gas  $a$ , while  $\phi_a = 1$  corresponds to gas  $b$ .

Table 2. Mixture parameter values in domains with homogeneous states

Parameter	Domain 1	Domain 2	Domain 3	Domain 4	Domain 5
$\rho$	1	1.9	2.7647	3.9581	2.5786
$u$	0	0	1.4833	0.9304	0.9304
$p$	1	1	4.4468	7.2498	7.2498
$\phi_a$	0	1	0	0	1

The computations were carried out until the time  $t_{fin} = 0.25$  on two grids ( $N = 500$  and  $N = 4000$ ) the same as in [10, 11]. The numerical results are shown in Fig. 4. A further mesh refinement does not affect the results. For the standard values of the artificial dissipative parameters  $Sc = Pr = 1$ , the total density profile exhibits a small dip at the interface caused by the excessive numerical smearing of the density component profiles. This defect was completely avoided by choosing suitable dissipation parameters, together with decreasing in the spatial mesh size of the difference scheme (see Fig. 4b). The best values of the dissipative parameters are  $\alpha = 0.5$ ,  $Sc = 0.3$ , and  $Pr = 5$ . Stable computations with these parameters are ensured at the maximum Courant number  $\beta = 0.25$ . Note that the shock waves are well resolved on the coarse grid, whereas the situation with the contact discontinuity is different. On the coarse grid in this domain ( $x \approx 0.57$ ) the profiles of both total density and its components exhibit nonmonotonicity. Additionally, a defect in the velocity profile is observed there. On the fine grid, these defects become hardly noticeable, which is well seen in Figs. 4b–4d.

The results of the QGD computations were found to be similar to both the self-similar solution and the data produced by the second-order accurate algorithms from [10] and [11].

### 5. RIEMANN PROBLEM FOR TWO DIFFERENT GAS MIXTURES

In the previous problems, the halves of the computational domain initially contained two different gases, while a gas mixture occupied only a small domain near the interface. Now, we consider the Riemann problem for gas mixtures with different component concentrations to the right and left of the discontinuity. The discontinuity initially is located at the point  $x = 0.5$ , separating mixtures of the same gases as in the preceding problem. Recall that the gas parameters are  $\gamma_a = 1.35$ ,  $C_{va} = 2.4$  and  $\gamma_b = 5.0$ ,  $C_{vb} = 1.5$ .

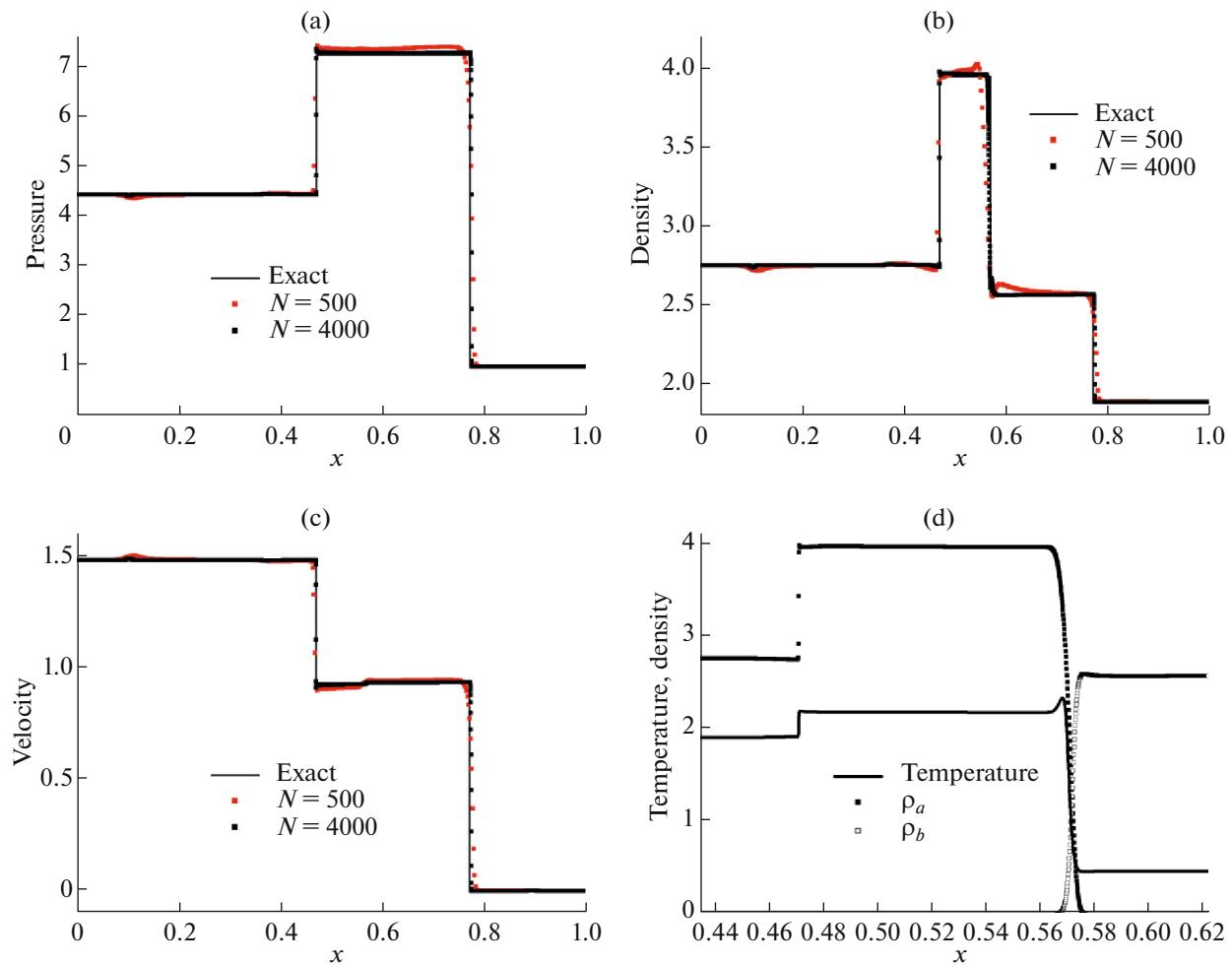


Fig. 4. Profiles of flow variables in the problem of the shock–interface interaction.

The initial conditions are specified as follows: the temperature in the entire computational domain is a constant equal to  $T_{\text{beg}} = 1.5$ , and the velocity is  $u_{\text{beg}} = 0$ . For  $x < 0.5$ , the densities of the components are  $\rho_a = 2$  and  $\rho_b = 1$ . To the right of the discontinuity (for  $x > 0.5$ ) the densities are  $\rho_a = 1$  and  $\rho_b = 0.2$ . Thus, the pressure to the left of the discontinuity is nearly four times higher than the pressure to the right of the discontinuity.

The computations were carried out until the time  $t_{\text{fin}} = 0.15$  with the following parameters of the scheme:  $\alpha = 0.5$ ,  $\beta = 0.2$ ,  $Sc = 0.4$ , and  $Pr = 1$ . The numerical results obtained on two spatial grids ( $N = 500$  and  $N = 5000$ ) are compared in Fig. 5, which clearly shows that the quality of the solution is improved under the mesh refinement.

This problem has no analytical solution. However, its formulation implies that a shock and a rarefaction wave should propagate rightward and leftward, respectively. Between them, there is a contact discontinuity. All these characteristic features are fairly well resolved even on the coarse grid with  $N = 500$ .

## 6. SIMULATION OF TWO-PHASE GAS–LIQUID MIXTURE

The numerical algorithm proposed in the first sections of this paper was generalized to the gas–liquid interaction in the approximation when the liquid is described by the stiffened gas model (see, e.g., [9, 18–20], and numerous references therein).

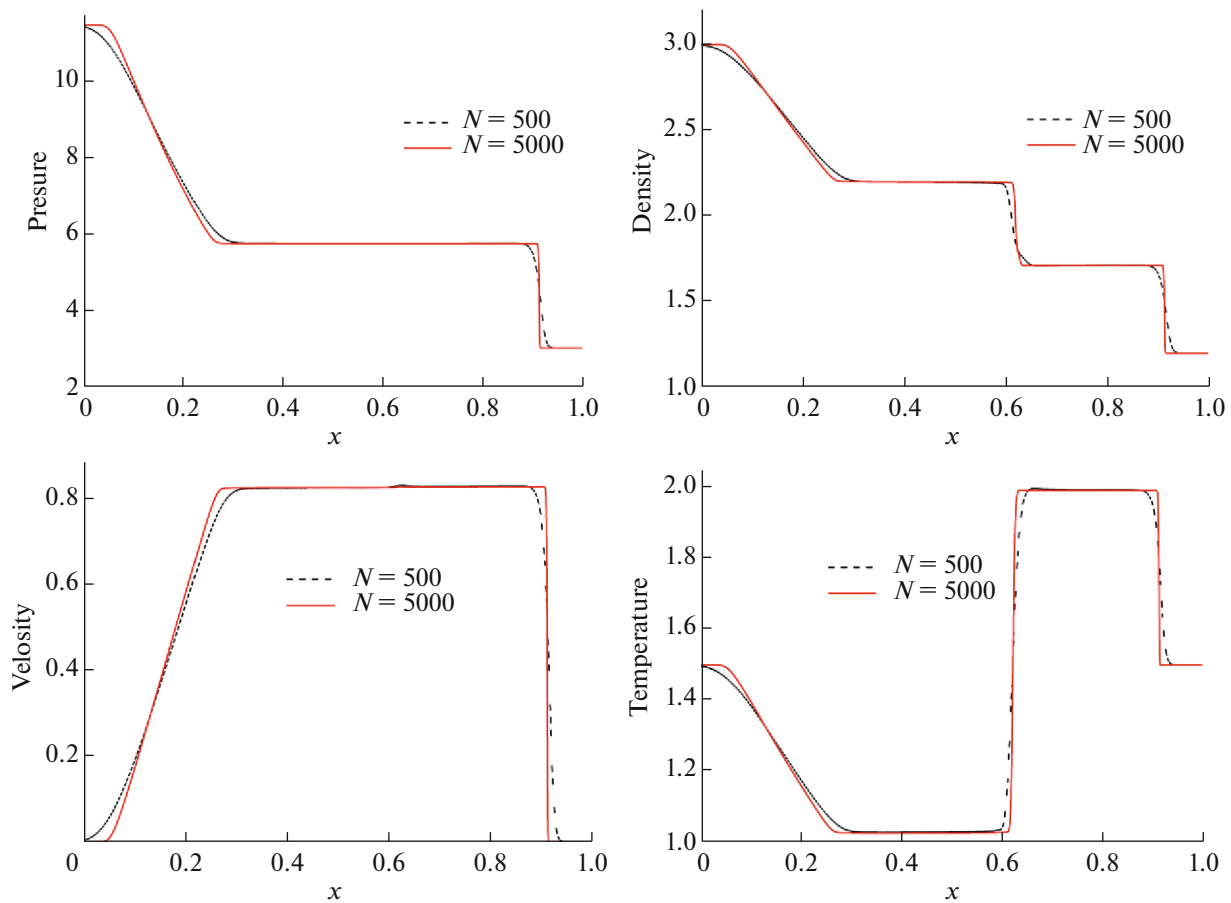


Fig. 5. Riemann problem for two mixtures.

This approximation is based on a modification of the equation of state for the liquid component. Specifically, the ideal gas law is supplemented with an additional term obtained by simplifying a Van der Waals type equation of state. The corresponding formulas are written according to [19] as follows:

$$p_k = \rho_k R_k T - p_{k\infty}, \quad \varepsilon_k = C_{V_k} T + \frac{p_{k\infty}}{\rho_k}, \quad k = a, b.$$

The additions to the pressure are chosen so as to ensure the necessary speed of sound in the liquid. For gases, the additions to the pressure are set to zero.

The total speed of sound is computed using the formula

$$\rho c_s^2 = \gamma_a(p_a + p_{a\infty}) + \gamma_b(p_b + p_{b\infty}).$$

The equations of state of the mixture are modified as follows:

$$\rho \varepsilon = T(\rho_a C_{V_a} + \rho_b C_{V_b}) + p_{\infty}, \quad p_{\infty} = \frac{\rho_a p_{a\infty} + \rho_b p_{b\infty}}{\rho}.$$

Our variant of computing  $p_{\infty}$  in the form of a weighted value of the pressures proves to be effective for mixtures with domains of zero densities of the component  $a$  or  $b$ .

According to [19], for air and water, the corresponding quantities have the following values:

—air (component  $a$ ):  $\gamma = 1.4$ ,  $C_p = 1004.5$  (J/(Kg K)),  $p_{a\infty} = 0$  (Pa).

—water (component  $b$ ):  $\gamma = 2.8$ ,  $C_p = 4186$  (J/(Kg K)),  $p_{b\infty} = 8.5 \times 10^8$  (Pa).

As an example, we present the numerical results obtained for the Riemann problem in the air–water medium. The problem was solved in the formulation described in [19].

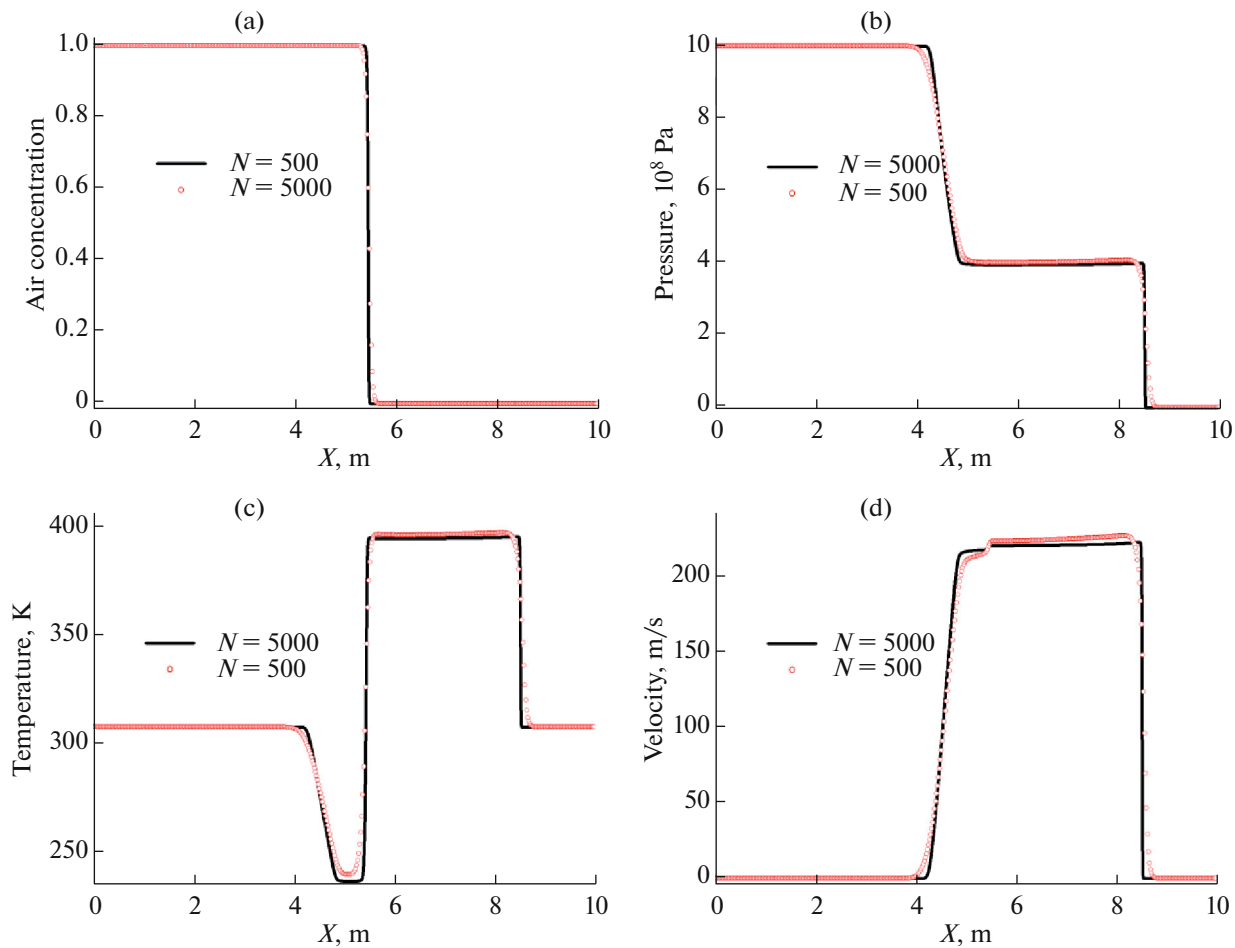


Fig. 6. Riemann problem in the air–water medium.

According to [19], the following initial conditions were specified in the computational domain  $0 \leq x \leq 10$  m:

$$\begin{aligned} (p, U, T)_{\text{air}} &= (10^9 \text{ Pa}, 0, 308.15 \text{ K}), \quad \rho_{\text{water}} = 0 \quad \text{for } x \leq 5 \text{ m}, \\ (p, U, T)_{\text{water}} &= (10^5 \text{ Pa}, 0, 308.15 \text{ K}), \quad \rho_{\text{air}} = 0 \quad \text{for } x > 5 \text{ m}. \end{aligned}$$

The computations were performed on grids with 500 and 5000 nodes until the time  $t_{\text{fin}} = 0.002$  s.

The best values of the dissipative regularization parameters were  $\alpha = 0.5$ ,  $Sc = 1$ , and  $Pr = 4$ . Stable computations with these parameters were ensured at the maximum Courant number  $\beta = 0.2$ . The spatial mesh sizes were equal  $h = 0.02$  and  $0.002$  m, respectively. The time steps were about  $2 \times 10^{-6}$  and  $2 \times 10^{-7}$  s, respectively.

The numerical results obtained on the 500 and 5000 grids are displayed in Figs. 6 and 7.

The presented distributions exhibit the characteristic features of the flow, namely, the rarefaction wave in the air in the  $x$  zone from 4 to 5 m, the air–water interface for  $x \sim 5.5$  m, and the shock wave in the water for  $x \sim 8.5$  m. It is well seen that the results obtained on the grids of 500 and 5000 nodes differ rather little, which suggests that the algorithm has good accuracy. Note that the results agree well with those from [19], although a high-order accurate method was used in [19], while the QGD algorithm is formally first-order accurate in time and space.

Additionally, Fig. 8 demonstrates the convergence of the numerical solution under mesh refinement up to 20 000 nodes. The figure presents a fragment of the velocity distribution with most noticeable differences in the numerical results. It can be seen that the unphysical step in the velocity distribution within the water–air interaction zone is smoothed out as the spatial step size decreases.

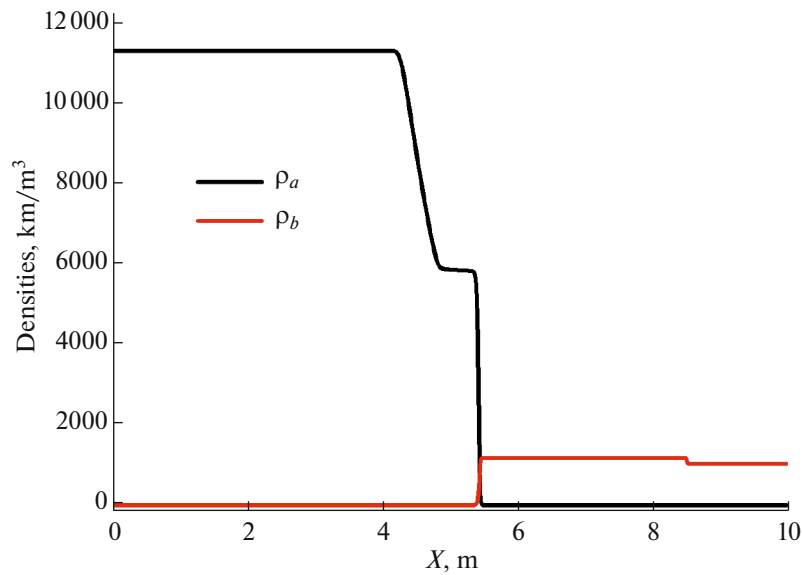


Fig. 7. Densities of the components ( $N = 5000$ ).

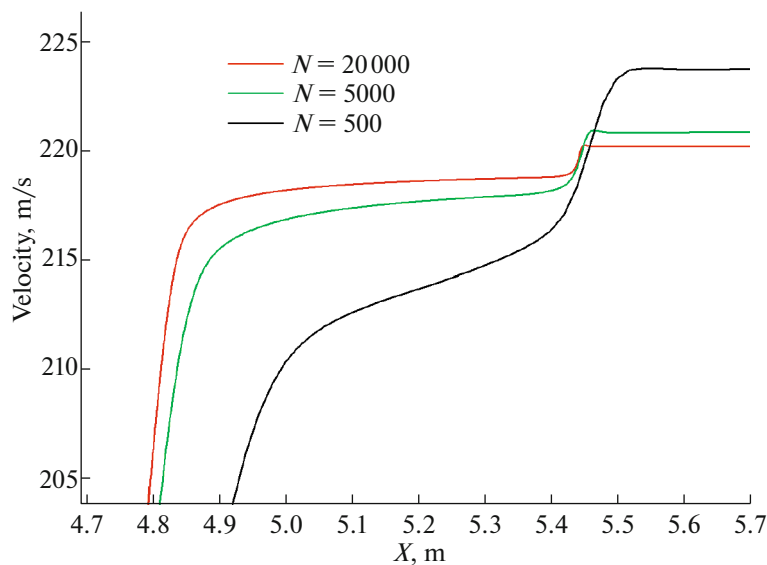


Fig. 8. Grid convergence of the algorithm. Fragment of the velocity distribution.

As the air pressure at the discontinuity decreases, the numerical experiments show that the instability of the velocity at the interface grows, as can be seen in Fig. 8, which then leads to the instability of the computation of the whole problem.

The numerical experiments and an analysis of the algorithm showed that a stable numerical solution in the simulation of a gas–liquid mixture can be obtained if the gas pressure is on the order or higher than the additional pressure in the liquid:

$$p_a \geq p_{b\infty}. \tag{21}$$

If condition (21) holds and the components have an identical pressure at the gas–liquid interface, then, in the numerical computation, the boundary of the contact discontinuity does not move, the flow velocities remain strictly zero, and the boundary is smeared by artificial viscosity over one spatial grid cell.

If relation (21) does not hold, then the numerical solution becomes unstable, which is associated with the simplified description of the liquid with the help of the two-term Van der Waals equation.

When the problem is solved numerically with low gas pressure values for which condition (21) does not hold, the value of  $p_{b\infty}$  can be reduced artificially. However, a decrease in  $p_{b\infty}$  leads to an unphysically low speed of sound in the liquid, the flow computation remains stable, but its results are inadequate.

## CONCLUSIONS

An extremely simple mathematical approach to flow simulation for a mixture of widely different fluids has been presented. The mixture flow is described by transport equations for the densities of the components and for the total velocity and temperature of the mixture. The temperatures and velocities of the components are assumed to be identical. The interface between the components is not identified explicitly.

For gas mixture flows, by applying the given algorithm, a supersonic unsteady flow with components having widely different ratios of specific heats was simulated without exhibiting numerical oscillations of gas component densities in the zone of their small values.

To compute flows of immiscible fluids of the gas–liquid type, the method was modified by applying a simplified Van der Waals equation of state. As a result, the computations could be performed without explicit identification of the interface, provided that the relation between the gas pressure and the addition determining the speed of sound in the liquid is satisfied.

The accuracy of the QGD computation varies depending on the regularization coefficients  $\alpha$ ,  $Sc$ , and  $Pr$ . With a suitable choice (tuning) of these coefficients, the accuracy approaches the one of a second-order scheme. The results of the QGD computations with suitably chosen dissipative coefficients were found close to the self-similar solution and data produced by second-order accurate algorithms (see [10, 11, 19]). The method demonstrates grid convergence.

As a further development of the described approach, the artificial viscosity and thermal conductivity of the mixture can be replaced by their actual values with the preservation of the regularizing QGD additions. By analogy with QGD algorithms available for one-component gases, the described method was generalized to multidimensional flows and unstructured meshes in its implementation within the OpenFOAM platform (see [14]).

## CONFLICT OF INTEREST

The authors declare that they have no conflicts of interest.

## REFERENCES

1. E. M. Lifshitz and L. P. Pitaevskii, *Physical Kinetics* (Pergamon, Oxford, 1981).
2. Ya. B. Zel'dovich and Yu. P. Raizer, *Physics of Shock Waves and High-Temperature Hydrodynamic Phenomena* (Dover, New York, 2002).
3. Yu. P. Golovachev, *Numerical Simulation of Viscous Gas Flows in Shock Layers* (Nauka, Moscow, 1996) [in Russian].
4. T. G. Elizarova, *Quasi-Gas Dynamic Equations* (Nauchnyi Mir, Moscow, 2007; Springer, Berlin, 2009).
5. T. G. Elizarova, A. A. Zlotnik, and E. V. Shil'nikov, "Regularized equations for numerical simulation of flows of homogeneous binary mixtures of viscous compressible gases," *Comput. Math. Math. Phys.* **59** (11), 1832–1847 (2019).  
<https://doi.org/10.1134/S0965542519110058>
6. T. G. Elizarova and E. V. Shil'nikov, "Numerical simulation of gas mixtures based on the quasi-gasdynamic approach as applied to the interaction of shock wave with a gas bubble," *Comput. Math. Math. Phys.* **61** (1), 118–128 (2021).  
<https://doi.org/10.1134/S096554252101004>
7. E. V. Shilnikov and T. G. Elizarova, "About one numerical method of compressible multifluid flow modelling in Euler formulation," in *Proceedings of IRF2020: 7th International Conference on Integrity–Reliability–Failure*, Ed. by J. F. Silva Gomes and S. A. Meguid (INEGI-FEUP, 2020), pp. 613–622.
8. I. R. Khaytaliev and E. V. Shilnikov, Preprint No. 52, IPM RAN (Keldysh Inst. of Applied Mathematics, Russian Academy of Sciences, Moscow, 2021).
9. R. Abgrall and S. Karni, "Computations of compressible multifluids," *J. Comput. Phys.* **169** (2), 594–623 (2001).

10. J. W. Banks, D. W. Schwendeman, A. K. Karila, and W. D. Henshaw, “A high-resolution Godunov method for compressible multi-material flow on overlapping grids,” *J. Comput. Phys.* **223** (1), 262–297 (2007).
11. V. E. Borisov and Yu. G. Rykov, “Modified Godunov method for multicomponent flow simulation,” *J. Phys.: Conf. Ser.* **1250**, 012006 (2019).  
<https://doi.org/10.1088/1742-6596/1250/1/012006>
12. V. E. Borisov and Yu. G. Rykov, “Simulation of multicomponent gas flows using the double-flux method,” *Math. Models Comput. Simul.* **13** (3), 453–465 (2021).
13. A. Zlotnik, A. Fedchenko, and T. Lomonosov, “Entropy correct spatial discretizations for 1D regularized systems of equations for gas mixture dynamics,” *Symmetry* **14**, 2171 (2022).  
<https://doi.org/10.3390/sym14102171>
14. [github.com/unicfdlab/QGDsolver](https://github.com/unicfdlab/QGDsolver)
15. M. V. Kraposhin, E. V. Smirnova, T. G. Elizarova, and M. A. Istomina, “Development of a new OpenFOAM solver using regularized gas dynamic equations,” *Comput. Fluids* **166**, 163–175 (2018).  
<https://doi.org/10.1016/j.compfluid.2018.02.010>
16. T. G. Elizarova, “Time averaging as an approximate technique for constructing quasi-gasdynamic and quasi-hydrodynamic equations,” *Comput. Math. Math. Phys.* **51** (11), 1973–1982 (2011).
17. Yu. V. Sheretov, *Continuum Dynamics under Spatiotemporal Averaging* (Regulyarnaya i Khaoticheskaya Dinamika, Moscow–Izhevsk, 2009) [in Russian].
18. F. Denner, C.-N. Xiao, and B. G. M. van Wachem, “Pressure-based algorithm for compressible interfacial flows with acoustically-conservative interface discretization,” *J. Comput. Phys.* **367**, 192–234 (2018).  
<https://doi.org/10.1016/j.jcp.2018.04.028>
19. K. Kitamura, M.-S. Liou, and C.-H. Chang, “Extension and comparative study of AUSM-family schemes for compressible multiphase flow simulations,” *Commun. Comput. Phys.* **16** (3), 632–674 (2014).  
<https://doi.org/10.4208/cicp.020813.190214a>
20. M.-S. Liou, C. Chang, L. H. Nguyen, and T. G. Theofanous, “How to solve compressible multifluid equations: A simple, robust and accurate method,” *AIAA J.* **46**, 2345–2356 (2007).

*Translated by I. Ruzanova*